Connectivity effects in the segmental self- and cross-reorientation of unentangled polymer melts

A. Ottochian,[1] D. Molin,[1,a)] A. Barbieri,[1,2,b)] and D. Leporini[1,3,c)]
[1]*Dipartimento di Fisica "Enrico Fermi," Università di Pisa, Largo B. Pontecorvo 3, I-56127 Pisa, Italy*
[2]*INFN, Sezione di Pisa, Largo B. Pontecorvo 3, I-56127 Pisa, Italy*
[3]*INFM-CRS SOFT, Largo B. Pontecorvo 3, I-56127 Pisa, Italy*

(Received 6 July 2009; accepted 19 October 2009; published online 6 November 2009)

The segmental (bond) rotational dynamics in a polymer melt of unentangled, linear bead-spring chains is studied by molecular dynamics simulations. To single out the connectivity effects, states with limited deviations from the Gaussian behavior of the linear displacement are considered. Both the self and the cross bond-bond correlations with rank $\ell=1,2$ are studied in detail. For $\ell=1$ the correlation functions are precisely described by expressions involving the correlation functions of the chain modes. Several approximations concerning both the self- and the cross-correlations with $\ell=1,2$ are developed and assessed. It is found that the simplified description of the excluded volume static effects derived elsewhere [D. Molin *et al.*, J. Phys.: Condens. Matter **18**, 7543 (2006)] well accounts for the short time cross-correlations. It also allows a proper modification of the Rouse theory which provides quantitative account of the intermediate and the long time decay of the rotational correlations with $\ell=1$. © *2009 American Institute of Physics*. [doi:10.1063/1.3262307]

I. INTRODUCTION

The rotational dynamics of polymers are currently studied by several experimental techniques, including dielectric relaxation,[1] NMR,[2] electron paramagnetic resonance,[3] light scattering,[4] and more recently, single molecule spectroscopies[5] and simulations.[6–18] Due to the computational effort, numerical studies often consider short, unentangled chains with dynamics which in the melt state is usually rationalized by the Rouse model.[19] Even if several papers discussed the rotational self-correlation functions, to the best of our knowledge only a few ones touched on the issue of the rotational *cross*-correlations, i.e., the ones involving *distinct* chain portions, in the framework of studies on dielectric relaxation,[14] the crossover from Rouse[19] to reptation dynamics,[16] local ordering effects,[15] and long-range bond-bond correlations.[6] This is a little bit surprising in that rotational cross-correlations with ℓ rank are involved in the interaction between dipoles placed on distinct parts of the polymeric chain, an issue of remarkable interest in dielectric relaxation ($\ell=1$) and other techniques such as NMR,[2] electron paramagnetic resonance,[3] light scattering,[4] and single molecule spectroscopies[20,21] ($\ell=2$).

Motivated by the above remarks, the present paper reports on extensive molecular dynamics (MD) simulations of melts of unentangled polymer chains with different lengths to the purpose of assessing the Rouse model as a convenient framework to interpret the rotational self- and cross-correlations with $\ell=1,2$. To better evidence the role of connectivity, a key concept of the Rouse model, we limited other effects like the heterogeneity of motion by carrying out the simulations under conditions of limited deviations from the Gaussian behavior of the linear displacement.

The paper is organized as follows. In Sec. II the Rouse model and the relevant predictions are presented. In Sec. III the relevant rotational correlation functions are defined. In Sec. IV the model and the details of the simulation are given. In Sec. V the results are discussed. In Sec. VI the conclusions are summarized.

II. SHORT ACCOUNT OF THE DISCRETE ROUSE MODEL

The Rouse model[19] is the simplest bead-spring model for flexible polymer chains.[22–24] It is usually applied to describe the long time or large scale dynamics of polymers by neglecting hydrodynamic interactions, chain entanglements, as well as excluded volume effects. This model has been frequently applied to nonentangled chains in concentrated solutions. It also serves in the description of the entangled chains: the tube model analyses the motion of the Rouse chain confined in a tubelike regime for calculating various kinds of dynamic properties.[23] Thus, the Rouse model is one of the most important models in the field of polymer dynamics and has been tested by experiments[25–31] and numerical simulations.[7–16,32–44] In particular, the Rouse dynamics of isotopic mixtures,[41] in confined environments,[13] and chemically reacting systems[44] have been studied. Corrections for free-volume effects,[39] intra- and intermolecular mean-force potentials[33] and uncrossability constraints[43] are also known. A mode-coupling theory providing microscopic justification for the use of the Rouse theory in polymer melts has been

a)Present address: Centro interdipartimentale di Fluidodinamica e Idraulica, Dip. di Energetica e Macchine, Universitá degli Studi di Udine, Via delle Scienze 208, I-33100 Udine, Italy.
b)Present address: Unconventional Reservoir Technologies (TENC)—ENI E & P Division, Via Emilia 1, I-20097 San Donato Milanese, Italy.
c)Electronic mail: dino.leporini@df.unipi.it.

developed.[45] Numerical simulations of polymer melts, to be compared with basic predictions of the mode-coupling theory, were also reported.[42]

In the discrete[46,47] Rouse model each chain is composed of M_R-1 segments being modeled by M_R noninteracting beads, connected by entropic springs with force constant $\kappa = 3k_BT/a_R^2$, where a_R is the average size of the segment, i.e., the root mean-square length of the spring, k_B is the Boltzmann constant, and T is the absolute temperature. No other interaction between the beads is present. The model considers a given chain and regards the surrounding ones as a uniform frictional medium with Gaussian properties. The segmental friction coefficient of the tagged chain is denoted by ζ. The surrounding chains are depicted to exert on each bead of the selected chain also a fast-fluctuating random force to ensure proper equilibrium properties via the fluctuation-dissipation theorem. The mean-field description of the Rouse model may be understood by noting that the size of a chain in the melt scales as $R_g^2 \propto M$, where R_g is the gyration radius and M is the number of monomers. If the monomer density of the melt is ρ, the number of chains N_c in the volume R_g scales as $N_c \propto \rho R_g^3/M \propto \sqrt{M}$.[33,34]

The Langevin equation for the inner beads of the tagged chain $(2 \le n \le M_R-1)$ is

$$\zeta \dot{\mathbf{r}}_n(t) = \frac{3k_BT}{a_R^2}[\mathbf{r}_{n-1}(t) - 2\mathbf{r}_n(t) + \mathbf{r}_{n+1}(t)] + \mathbf{f}_n(t), \tag{1}$$

and for the end beads $(n=1, M_R)$

$$\zeta \dot{\mathbf{r}}_1(t) = \frac{3k_BT}{a_R^2}[\mathbf{r}_2(t) - \mathbf{r}_1(t)] + \mathbf{f}_1(t), \tag{2}$$

$$\zeta \dot{\mathbf{r}}_{M_R}(t) = \frac{3k_BT}{a_R^2}[\mathbf{r}_{M_R-1}(t) - \mathbf{r}_{M_R}(t)] + \mathbf{f}_{M_R}(t), \tag{3}$$

where $\mathbf{r}_n$ is the position vector of the nth bead of the chain and the dot denotes a time derivative. The Cartesian components of the stochastic force $\mathbf{f}_n(t)$ are modeled as Gaussian white noise with zero average and correlations according to the fluctuation-dissipation theorem

$$\langle f_{n\alpha}(t) f_{m\beta}(t') \rangle = 2\zeta k_B T \delta_{nm} \delta_{\alpha\beta} \delta(t-t'). \tag{4}$$

The set of Eq. (1) with $n=1, \ldots, M_R$ are exactly solvable.[47] The solution, i.e., the position of the nth bead $\mathbf{r}_n$, is conveniently expressed in terms of normal coordinates, the so-called Rouse modes $\mathbf{X}_p^R$ with $p=0, \ldots, M_R-1$, as

$$\mathbf{r}_n(t) = \mathbf{X}_0^R(t) + 2\sum_{p=1}^{M_R-1} \mathbf{X}_p^R(t) \cos\left[\frac{(n-1/2)p\pi}{M_R}\right]. \tag{5}$$

The Rouse modes may be conversely written as

$$\mathbf{X}_p^R(t) = \frac{1}{M_R}\sum_{n=1}^{M_R} \mathbf{r}_n(t) \cos\left[\frac{(n-1/2)p\pi}{M_R}\right]. \tag{6}$$

The static cross-correlations between the Rouse modes vanish. In particular, for $p>0$

$$\langle \mathbf{X}_p^R \cdot \mathbf{X}_q^R \rangle = \delta_{pq} \frac{a_R^2}{8M_R \sin^2(p\pi/2M_R)}, \tag{7}$$

$$\cong \delta_{pq} \frac{M_R a_R^2}{2\pi^2 p^2}, \quad p/M_R \ll 1. \tag{8}$$

For $p, q=0$ one finds

$$\langle |\mathbf{X}_0^R(t) - \mathbf{X}_0^R(0)|^2 \rangle = 6\frac{k_BT}{M_R\zeta} t, \tag{9}$$

which describes the diffusive motion of the center of mass $\mathbf{R}_{CM} = \mathbf{X}_0^R$. For $p>0$, having defined the normalized self-correlation function of the pth Rouse mode as

$$\phi_p^R(t) = \frac{\langle \mathbf{X}_p^R(t) \cdot \mathbf{X}_p^R(0) \rangle}{\langle |\mathbf{X}_p^R|^2 \rangle}. \tag{10}$$

The Rouse model predicts the exponential decay of $\phi_p^R(t)$

$$\phi_p^R(t) = \exp\left[-\frac{t}{\tau_p}\right], \tag{11}$$

with characteristic time

$$\tau_p = \frac{\zeta a_R^2}{12k_BT \sin^2(p\pi/2M_R)}, \tag{12}$$

$$\cong \frac{\zeta a_R^2}{3\pi^2 k_BT} \frac{M_R^2}{p^2}, \quad p/M_R \ll 1. \tag{13}$$

III. ROTATIONAL CORRELATION FUNCTIONS

In this section suitable correlation functions to characterize both the global and the local reorientation of the chain are defined and some approximations presented. The corresponding Rouse expressions are identified.

A. Bond correlation functions

1. Definitions

One is interested in the rotational dynamics of linear polymer chains with M stiff monomers, the mth one being located at the position $\mathbf{R}_m$, $1 \le m \le M$. The local reorientation process is accounted for by the unit vector along the mth bond of the chain $\mathbf{b}_m$ as

$$\mathbf{b}_m = \frac{1}{b_0}(\mathbf{R}_{m+1} - \mathbf{R}_m), \tag{14}$$

b_0 being the bond length. The rotational self-correlation function of the nth bond with rank ℓ is defined as

$$C_{\ell,n}(t) = \langle P_\ell(\mathbf{b}_n(t) \cdot \mathbf{b}_n(0)) \rangle, \tag{15}$$

where $P_\ell(x)$ is the Legendre polynomial of order ℓ. The self-correlation function averaged over all the bonds is defined as

$$C_\ell(t) = \frac{1}{M-1}\sum_{n=1}^{M-1} C_{\ell,n}(t). \tag{16}$$

In order to consider the rotational cross-correlation function between the mth and $(m+\Delta m)$th bond, one defines

$$\chi(t) = \mathbf{b}_{m+\Delta m}(t) \cdot \mathbf{b}_m(0). \tag{17}$$

The rotational cross-correlation function with rank $\ell=1$ between the mth and $(m+\Delta m)$th bonds is defined as

$$C_{1,m,\Delta m}(t) = \langle \chi(t) \rangle, \tag{18}$$

whereas the rotational cross-correlation function with rank $\ell=2$ is defined as

$$C_{2,m,\Delta m}(t) = \langle \chi^2(t) \rangle - \tfrac{1}{3}. \tag{19}$$

Note that for $\Delta m \neq 0$, $C_{1,m,\Delta m}(0)$ and $C_{2,m,\Delta m}(0)$ have no trivial values due to excluded volume effects. However, they both vanish at long times, i.e., $C_{1,m,\Delta m}(\infty)=C_{2,m,\Delta m}(\infty)=0$. We also note that $C_{1,m,0}(t)=C_{1,m}(t)$ and $C_{2,m,0}(t)=2C_{2,m}(t)/3$.

The cross-correlation function averaged over all the bonds which are spaced by $\Delta m-1$ other segments is defined as

$$C_{\ell,\Delta m}(t) = \frac{1}{M-1-\Delta m} \sum_{m=1}^{M-1-\Delta m} C_{\ell,m,\Delta m}(t). \tag{20}$$

2. Approximations

Equation (15) yields $C_{\ell,n}(t) \simeq 1-\ell(\ell+1)\langle \theta_n^2(t) \rangle/4$ at short times, where $\theta_n(t)$ is the angle spanned by the bond $\mathbf{b}_n$ in a time t. At short times the chain connectivity little affects the bond reorientation. Then, one anticipates that the initial stage of the correlation loss is well accounted for by the *free* rotational diffusion which predicts $C_{\ell,n}(t)=\exp[-\ell(\ell+1)D_r t]$ at *any* time, thus leading to the identification $\langle \theta_n^2(t) \rangle = 4D_r t$, D_r being the rotational diffusion coefficient.[48] Even if the linear increase in time does not hold at long times in that $\langle \theta_n^2(\infty) \rangle = (\pi^2-4)/2$, the following ansatz will be considered:

$$C_{\ell,n}(t) \simeq \exp\left[-\frac{\ell(\ell+1)}{4} \langle \theta_n^2(t) \rangle \right]. \tag{21}$$

The above approximation is expected to hold for correlation functions with high ℓ-values decaying on shorter time scales. If one neglects the weak dependence of $\langle \theta_n^2(t) \rangle$ on the bond number n, Eq. (21) reduces to

$$C_{\ell}(t) \simeq \exp\left[-\frac{\ell(\ell+1)}{4} \langle \theta^2(t) \rangle \right], \tag{22}$$

where $\langle \theta^2(t) \rangle$ is the average of $\langle \theta_n^2(t) \rangle$ over all the bonds. Equation (21) predicts $C_{2,n}(t)=C_{1,n}(t)^3$ so that, by using Eqs. (16), for $\ell=2$

$$C_2(t) \simeq \frac{1}{M-1} \sum_{n=1}^{M-1} C_{1,n}(t)^3. \tag{23}$$

The above approximation is expected to improve Eq. (22) with $\ell=2$ since it has the correct limit $C_2(\infty)=0$. Note that Eqs. (21)–(23) do not necessarily imply an exponential time decay.

Another relation may be written for the cross-correlation functions as well. Let us consider the angle $\beta_{m,\Delta m}$ between $\mathbf{b}_m(0)$ and $\mathbf{b}_{m+\Delta m}(0)$ and the angle $\phi_{m,\Delta m}(t)$ between the two vectors $\mathbf{b}_{m+\Delta m}(0)\times\mathbf{b}_m(0)$ and $\mathbf{b}_{m+\Delta m}(0)\times\mathbf{b}_{m+\Delta m}(t)$, respectively [$\phi_{m,\Delta m}(t)$ is the dihedral angle of the two planes with the two vectors as normal vectors]. If both $\theta_{m+\Delta m}$ and $\phi_{m,\Delta m}$ are weakly correlated with $\beta_{m,\Delta m}$(roughly, this means that the static correlations between two bonds spaced by Δm do not affect their dynamics), $C_{1,m,\Delta m}(t)$ is approximated by

$$C_{1,m,\Delta m}(t) \simeq \langle \cos \beta_{m,\Delta m} \rangle \langle \cos \theta_{m+\Delta m}(t) \rangle + \langle \sin \beta_{m,\Delta m} \rangle \langle \sin \theta_{m+\Delta m}(t) \cos \phi_{m,\Delta m}(t) \rangle. \tag{24}$$

Notice that $\langle \cos \theta_{m+\Delta m}(t) \rangle = C_{1,m+\Delta m}(t)$ and that the angle $\beta_{m,\Delta m}$ calculation requires only information on statistics.

B. Rouse segment correlation functions

1. Definitions and properties

To assess the predictions of the Rouse model on the rotational dynamics, suitable correlation functions to be compared with the ones of Sec. III A 1 must be defined. Henceforth, for a given correlation function C, the corresponding Rouse expression will be denoted by C^R. Their relations with the modes $\mathbf{X}_p^R$ are given in the Appendix.

To characterize the local reorientation of the chain one has to focus on the correlation functions of the Rouse segments to be defined as

$$\mathbf{a}_n = \frac{1}{a_R}(\mathbf{r}_{n+1} - \mathbf{r}_n), \quad n = 1, \ldots, M_R - 1. \tag{25}$$

One aspect to be considered is that, differently from bonds, the length of the segments of the Rouse chain is Gaussian distributed and the moments only are known, e.g.

$$\langle a_n^2 \rangle = 1, \tag{26}$$

$$\langle a_n^4 \rangle = \tfrac{5}{3}, \tag{27}$$

with $a_n^2 \equiv \mathbf{a}_n \cdot \mathbf{a}_n$.

The rotational self-correlation function of the nth segment with rank $\ell=1$ is defined as

$$C_{1,n}^R(t) = \langle \mathbf{a}_n(t) \cdot \mathbf{a}_n(0) \rangle. \tag{28}$$

The above equation is formally identical to the corresponding bond-bond correlation function for fixed bond length b_0, i.e., Eq. (15) with $\ell=1$. Since $C_{1,n}^R(t)$ involves $\langle a_n^2 \rangle$ only, Eq. (28) is mapped into Eq. (15) by the identification $a_R=b_0$.[49–51]

If the correlation functions with rank $\ell \geq 2$ are considered, the moments $\langle a_n^{2p} \rangle$ with $p \geq 2$ come into play. Since the inequality $\langle a_n^{2p} \rangle \neq \langle a_n^2 \rangle^p = 1$ holds [e.g., see Eq. (27)], the correlation functions C^R with $\ell \geq 2$ must be properly defined for comparison with the corresponding ones of Sec. III A 1. Owing to that, the self-correlation function of the nth segment with rank $\ell=2$ is defined as

$$C_{2,n}^R(t) = \frac{3\langle [\mathbf{a}_n(t) \cdot \mathbf{a}_n(0)]^2 \rangle - 1}{4}. \tag{29}$$

With the above definitions $C_{\ell,n}^R(0)=1$ and $C_{\ell,n}^R(\infty)=0$. Note that $C_{2,n}^R$ and the corresponding bond correlation function, Eq. (15) with $\ell=2$, are formally different.

In analogy with Eq. (16) one defines the self-correlation function averaged over the M_R-1 segments as

$$C_\ell^R(t) = \frac{1}{M_R - 1} \sum_{n=1}^{M_R-1} C_{\ell,n}^R(t). \tag{30}$$

A compact expression for $C_1^R(t)$ is presented as Eq. (A7) in the Appendix. In the Appendix it is also shown that

$$C_{2,n}^R(t) = C_{1,n}^R(t)^2. \tag{31}$$

From Eq. (30) one gets

$$C_2^R(t) = \frac{1}{M_R - 1} \sum_{n=1}^{M_R-1} C_{1,n}^R(t)^2. \tag{32}$$

The cross-correlation functions are defined in terms of

$$\chi^R(t) = \mathbf{a}_{m+\Delta m}(t) \cdot \mathbf{a}_m(0). \tag{33}$$

The expressions of $C_{1,m,\Delta m}^R(t)$ and $C_{2,m,\Delta m}^R(t)$ are get by replacing $\chi(t)$ with $\chi^R(t)$ in Eqs. (18) and (19), respectively

$$C_{1,m,\Delta m}^R(t) = \langle \chi^R(t) \rangle, \tag{34}$$

$$C_{2,m,\Delta m}^R(t) = \langle [\chi^R(t)]^2 \rangle - \tfrac{1}{3}. \tag{35}$$

We note that $C_{1,m,0}^R(t) = C_{1,m}^R(t)$ and $C_{2,m,0}^R(t) = 4C_{2,m}^R(t)/3$. In Appendix it is shown that

$$C_{2,m,\Delta m}^R(t) = \tfrac{4}{3} C_{1,m,\Delta m}^R(t)^2. \tag{36}$$

The average of the cross-correlation functions over all the segments $C_{\ell,\Delta m}^R(t)$ and $\ell = 1,2$ is defined in analogy with Eq. (30).

By replacing Eq. (5) into Eq. (25) and inserting the result into Eqs. (28), (29), (34), and (35) the self-correlation and cross-correlation functions with rank $\ell = 1,2$ are related to the normalized correlation functions of the Rouse mode $\phi_p^R(t)$ [Eq. (11)]. Their explicit expressions are derived in the Appendix. In general, correlation functions with rank ℓ are expressed by multivariate polynomials with degree ℓ in terms of the variables $\phi_p^R(t)$ with $p = 1, \ldots, M_R - 1$.

Rouse chains are "phantom" chains, i.e., excluded volume effects are ignored. This means

$$\langle \mathbf{a}_m \cdot \mathbf{a}_{m+k} \rangle = \delta_{k0}. \tag{37}$$

The above relation sets the static properties of the Rouse modes, i.e., Eq. (7).[23] In this limit the cross-correlation functions at very short times vanish, i.e., $C_{\ell,m,\Delta m}^R(0) = 0$ for $\ell = 1,2$ and $\Delta m \neq 0$, as one may check in Eqs. (A4) and (A9) for $\ell = 1$, as well as Eq. (A14) for $\ell = 2$.

2. Approximation

In order to test the Rouse model one has to evaluate the modes $\mathbf{X}_p^R(t)$. To this aim, the bead position is identified with the monomer position in Eq. (6),

$$\mathbf{X}_p(t) = \frac{1}{M} \sum_{n=1}^{M} \mathbf{R}_n(t) \cos\left[\frac{(n - 1/2)p\pi}{M} \right]. \tag{38}$$

The key quantity of the Rouse expressions concerning the rotational correlation functions are the mode correlation functions $\langle \mathbf{X}_p(t) \cdot \mathbf{X}_p(0) \rangle$. A number of schemes for their evaluation will be adopted which are summarized by the relation

$$\langle \mathbf{X}_p(t) \cdot \mathbf{X}_p(0) \rangle = \langle |\mathbf{X}_p|^2 \rangle^i \phi_p(t), \quad i = \mathrm{MD}, \ R, \ \mathrm{SM3}, \tag{39}$$

where the normalized mode correlation function ϕ_p is taken from simulations (see examples in Fig. 2). The label $i = \mathrm{MD}$ means that the correlation function is evaluated from simulations in full. Setting $i = R$ implies that the modulus is taken by Eq. (7). The choice $i = \mathrm{SM3}$ signals that the modulus is evaluated from Eq. (38) according to the SM3 model.[52,53] The SM3 model removes the phantom character of the Rouse chains by providing excluded volume corrections to the single-chain static properties of a melt of unentangled polymers. It needs the temperature and the interaction potential between nonbonded monomers [Eq. (40) in the present work] as only input parameters.

IV. DETAILS OF THE SIMULATION

We investigate systems of N fully flexible linear chains with M monomers each. The (M,N) pairs under investigation are (3, 667), (5, 200), (10, 200), (15, 220), (22, 300) and, (30,300). The sample is confined into a cubic box with periodic boundary conditions. To handle the boundary conditions, the minimum image convention is adopted. The interaction between nonbonded monomers occurs via the Lennard-Jones (LJ) potential given by

$$U(r) = 4\epsilon[(\sigma/r)^{12} - (\sigma/r)^6] + U_{\mathrm{cut}}. \tag{40}$$

The potential is cut off at $r_{\mathrm{cut}} = 2.5\sigma$ and properly shifted by U_{cut} so as to vanish at that point and to make it continuous everywhere. No torsional potential is present. The RATTLE (Ref. 54) algorithm is used to constrain neighboring monomers in the same chain at a distance $b_0 = 0.97\sigma$. From now on LJ units are adopted with the Boltzmann constant $k_b = 1$. The samples are equilibrated under Nosé-Andersen[54] dynamics at a given temperature T and pressure P until the average displacement of the chains' centers of mass is as large as twice the mean end-to-end distance. Data are collected during production runs in microcanonical conditions. The time step for the chosen velocity verlet integration is $\delta t = 2.5 \times 10^{-3}$. No adjustment of the temperature, e.g., by rescaling the velocities, was needed during the production run. The results have been averaged over ten independent runs at least. The system is studied at constant pressure $P = 2.0$ and temperature $T = 1.2$ for chains with length $M = 3$, 5, 10, 15, 22, and 30, and at temperatures $T = 0.65$, 0.7, 0.75, 0.8, 1.0, 1.2, 1.4, 1.6, and 1.8 for the chain with $M = 10$.

V. RESULTS AND DISCUSSION

Flexible linear chains have average size of the segment $a_R = \sqrt{C_\infty} b_0$.[23,32] For the present case, i.e., fully flexible chains, the characteristic ratio $\sqrt{C_\infty} = 1.19$.[17] On this basis the identification $M_R = M$ is used when comparing the Rouse predictions with the numerical results and the Rouse modes are evaluated by Eq. (38). They are found to be fairly orthogonal. In fact, the quantity $\langle \mathbf{X}_p \cdot \mathbf{X}_q \rangle$ with $p \neq q$ is two to three orders of magnitude less than the moduli of the involved modes (data not shown) in agreement with other studies.[36]

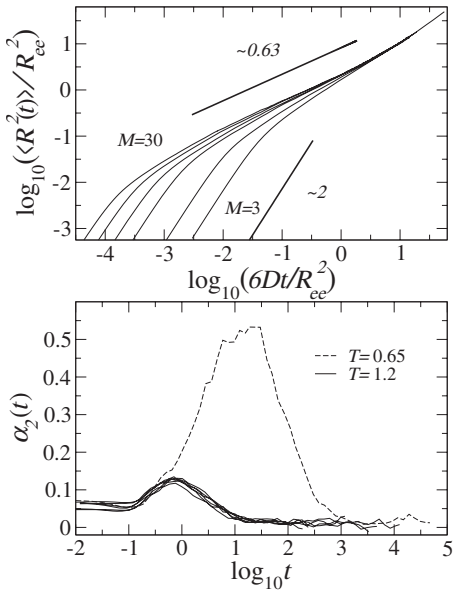

FIG. 1. Top: Scaled plot of the monomer mean-square displacement at $T=1.2$ for $M=3$, 5, 10, 15, 22, and 30 (from right to left). R_{ee}^2 denotes the mean-square end-to-end distance. The slopes of the ballistic and the intermediate-time regimes are also drawn. At long times (not shown) the displacements occur by the usual diffusion law $\langle R^2(t)\rangle=6Dt$ where D is the diffusion coefficient. Bottom: non-Gaussian parameter of the monomer displacement α_2 for $M=3$, 5, 10, 15, 22, and 30 at $T=1.2$ (solid lines) and $M=10$ at $T=0.65$ (dashed line).

A. Monomer displacement and Rouse modes

Figure 1 (top panel) shows the monomer mean-square displacement at $T=1.2$ for all the chain lengths under study. Curves are suitably scaled for easier comparison. A number of different regimes are seen. At short times ($t\lesssim 0.1$) the motion is ballistic: $\langle \mathbf{R}^2\rangle \propto t^2$. At later times the connectivity drives the motion of monomers to a subdiffusive regime, i.e., $\langle \mathbf{R}^2\rangle \propto t^x$ with $x\simeq 0.6<1$. The Rouse model predicts $x_R=0.5$.[23] For displacements larger than the mean-square end-to-end distance R_{ee}^2 (not shown in Fig. 1) the monomer motion becomes diffusive, i.e., $\langle \mathbf{R}^2\rangle=6Dt$ where D is the diffusion coefficient. Notice the absence of any plateaulike region in the mean-square displacements and then the missing evidence of well-defined caging effects due to nearest neighbors at $T=1.2$. Escaping from traps exhibits marked non-Gaussian features which may be characterized by the non-Gaussian parameter α_2 [17]

$$\alpha_2(t)=\frac{3}{5}\frac{\langle|\Delta\mathbf{R}(t)|^4\rangle}{\langle|\Delta\mathbf{R}(t)|^2\rangle^2}-1. \tag{41}$$

Figure 1 (bottom) plots α_2 for all the chain lengths under study at $T=1.2$ and for $M=10$ at $T=0.65$. The small deviations from the Gaussian behavior confirm the negligible trapping of the monomers at $T=1.2$. Differently, the decamer at $T=0.65$ exhibits somewhat larger deviations pointing to stronger caging of the monomers.

Figure 2 (top panel) plots the normalized self-correlation functions of the Rouse modes $\phi_p(t)$ for $M=10$ and $T=1.2$. The top inset evidences that $\phi_p(t)$ decays at long times as a stretched exponential with stretching parameter $\beta\sim 0.86$. The Rouse model predicts $\beta=1$ for all the modes [Eq. (11)].

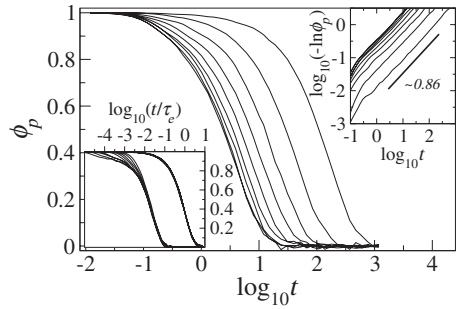

FIG. 2. Rouse modes for $M=10$. Self-correlation functions $\phi_p(t)$ at $T=1.2$. Top inset: log-log plot of the logarithm of $\phi_p(t)$. The decay at long times is a stretched exponential with stretching parameter $\beta\sim 0.86$ given by the slope of the solid line. Bottom inset: scaling of the slowest (ϕ_1) and the fastest (ϕ_9) correlation functions for $T=0.65$, 0.7, 0.75, 0.8, 1.2, 1.4, 1.6, and 1.8. Note the plateau region of $\phi_9(t)$ at short times and the lowest temperatures evidencing the cage effect. The latter is not seen in $\phi_1(t)$.

The discrepancy is known and ascribed to the limited allowable range of chain lengths to see the Rouse dynamics which, expectedly, yields finite M corrections to the ideal Rouse behavior.[13] The bottom inset of Fig. 2 shows a detailed view of the slowest ($p=1$) and the fastest ($p=9$) correlation functions of the Rouse modes for all the temperatures. Curves are scaled by τ_e, being defined by $\phi_1(\tau_e)=1/e$. The scaling works nicely for $\phi_1(t)$, whereas deviations are apparent at short times for $\phi_9(t)$ where at the lowest temperatures a plateau develops signaling the onset of the cage effect in agreement with the analysis of the non-Gaussian effects in Fig. 1 bottom. The plateau is not seen in $\phi_1(t)$ which has not relaxed appreciably within the cage lifetime. The larger sensitivity to caging of $\phi_9(t)$ is understood by noting that the mode $\mathbf{X}_9$ represents the local motion of the chain which includes $M/p=10/9\sim 1$ bonds.[23] The missing time/temperature scaling of the cage effect is well-known, e.g., see Ref. 55. Differently, the time/temperature scaling of the long-time relaxation is a major prediction of the Rouse model.[23]

B. Rotational self-correlation functions

Figure 3 shows the temperature-dependence of the rotational correlation function $C_\ell(t)$ [Eq. (16)] for $\ell=1,2$ of the melt of decamers ($M=10$). It is seen that at the same temperature $C_2(t)$ decays faster than $C_1(t)$ since the former is more sensitive to small angular displacements and the rotational dynamics is not dominated by jumps which would lead to substantial ℓ-independence of the decay times.[55] On decreasing the temperature, both $C_1(t)$ and $C_2(t)$ show a plateau at short times signaling the onset of the cage effect. As it is anticipated, the confined motion inside the cage results in larger correlation losses for $\ell=2$ than $\ell=1$. Figure 3 shows that $C_1(t)$ and $C_2(t)$ have several decay regimes well expressed by the general form $\log C(t)\propto -t^x$, the x exponent being dependent on the particular time window under consideration. At very short times in the ballistic regime $\langle\theta^2(t)\rangle\sim t^2$ and then $\log C_\ell(t)\sim -t^2$ according to Eq. (22). At longer times and low temperatures there is a crossover from ballistic to caged dynamics evidenced by the quasiplateau at $1\lesssim t\lesssim 10$. At higher temperatures the latter is not apparent.

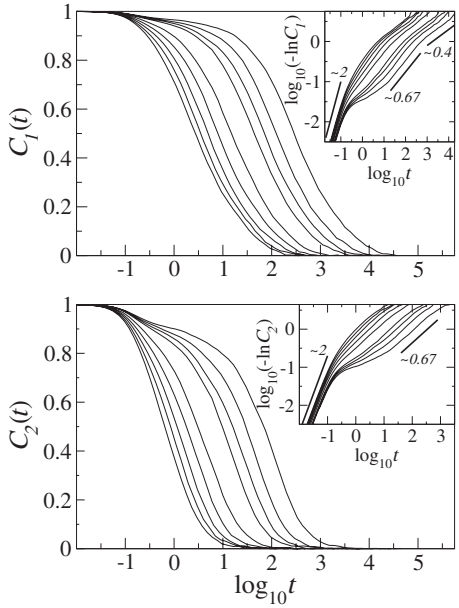

FIG. 3. Rotational correlation functions C_1 (top) and C_2 (bottom) for $M=10$ for all the investigated temperatures. Inset: log-log plot of the logarithm of the correlation function. Three distinct decay regimes according to the law $log\ C \sim -t^x$ are shown with the indicated x value.

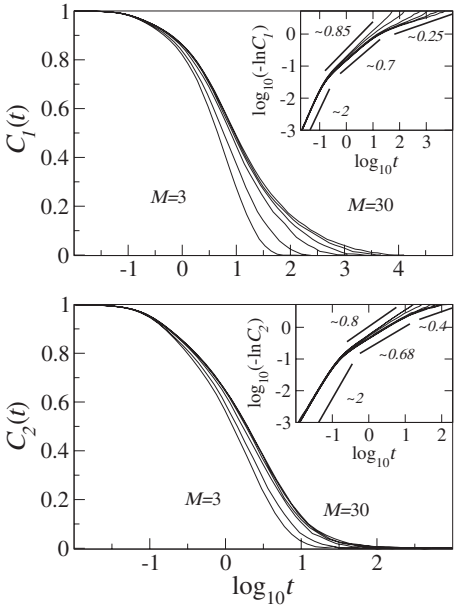

FIG. 5. Rotational correlation functions $C_1(t)$ (top) and $C_2(t)$ (bottom) at $T=1.2$ for $M=3$, 5, 10, 15, 22, and 30 (from left to right). The distinct decay regimes according to the law $log\ C \sim -t^x$ are shown in the insets with the indicated x value.

At longer times the rotational motion enters a new regime where the connectivity affects markedly the bond reorientation and leads to a stretched decay with stretching parameter $x \simeq 0.67$ for $\ell=1$ and 2. Notice that the parameter is quite close to the exponent of the subdiffusive regime of the mean-square displacement occurring in the same time window (see Fig. 1). At longer times $C_1(t)$ crosses over to a slower decay regime with stretching parameter $x' \sim 0.4$. Both stretching parameters do not exhibit appreciable temperature dependence, as it is seen in Fig. 4 where the curves are scaled by

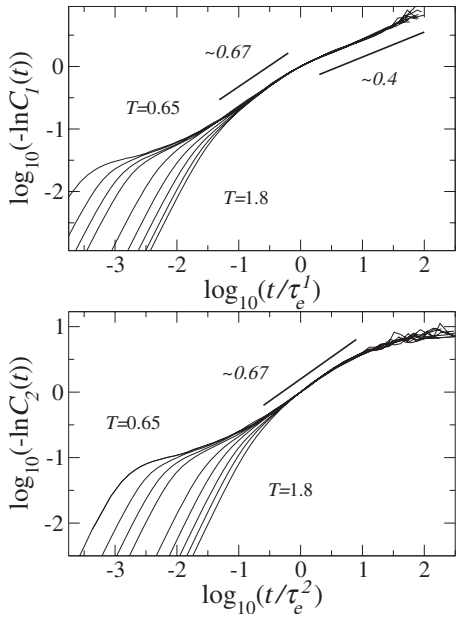

FIG. 4. Scaled curves of the rotational correlation function $C_1(t)$ (top) and $C_2(t)$ (bottom) of Fig. 3 for $M=10$ and all the investigated temperatures. Distinct decay regimes according to the law $log\ C \sim -t^x$ are shown with the indicated x value.

τ_e^ℓ, the latter being defined by $C_\ell(\tau_e^\ell)=1/e$. Equation (22) gives a hint about the similarity of the time-dependence of $C_1(t/\tau_e^1)$ and $C_2(t/\tau_e^2)$. It states that changing the ℓ rank just shifts $\log_{10}(-\ln C_{\ell,n})$ by a constant term. Notice that Fig. 4 also shows that both $C_1(t)$ and $C_2(t)$ are effectively scaled onto master curves at intermediate and long times but not at short times where caging is effective, in agreement with previous findings for both dimers[55] and decamers.[17]

Figure 5 shows the molecular weight dependence of $C_1(t)$ and $C_2(t)$ for $T=1.2$. It is seen that the decay is weakly dependent on the chain length for $1 \lesssim t \lesssim 10$ (intermediate times), whereas increasing the connectivity leads, especially for $C_1(t)$, to a slower decay for $t \gtrsim 10$ (long times). Insight into the time dependence of $C_1(t)$ is reached by numerical evaluation of Eq. (A6) via Eq. (39) with $i=$SM3 and

$$\phi_p(t) = \exp\left[-\left(\frac{t}{\tau_p^\star(M_R)}\right)^\beta\right], \tag{42}$$

with $\tau_p^\star(M_R)=\tau/\sin^2(p\pi/2M_R)$. Equation (42) assumes equal stretching for all the modes (see Fig. 2) and the SM3 model removes the phantom character of the Rouse chains (see Sec. III B 1). Figure 6 shows the results. It is seen that the x slope of the intermediate regime just reflects the stretching of the Rouse modes. The long-time regime takes place for $t \gtrsim \tau_1^\star(M_R)$. The larger stretching with increasing chain length is ascribed to the wider distribution of relaxation times $\tau_p^\star(M_R)$ spanning the range $1 \leq p \leq M_R-1$. Figure 5 shows that the decay of $C_2(t)$ exhibits two regimes with analogous features with respect to the ones of $C_1(t)$.

It is interesting to compare the decay of $C_1(t)$ and $C_2(t)$ with the approximations developed in Secs. III A 2 and III B 2 This is done in Figs. 7 and 8.

Figure 7 shows that $C_1(t)$ is virtually coincident with Eq. (A6) by using Eq. (38) to evaluate the Rouse mode correla-

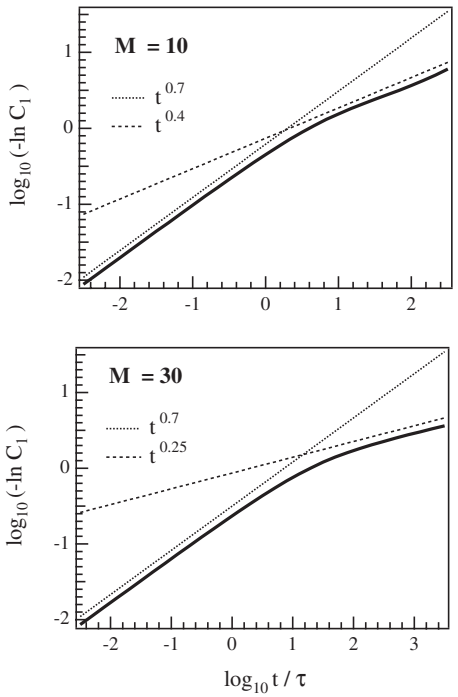

FIG. 6. Time dependence of $C_1(t)$ as evaluated by Eq. (A6) with Eq. (42) and $M_R=M$ and $\beta=0.7$. The plots account for the intermediate and long times decays of the chains with length $M=10$ (compared with Fig. 4 top) and $M=30$ (compared with the inset of Fig. 5 top)

tion functions from the MD data. The agreement is quite expected since Eq. (A6) follows from the high orthogonality of the modes $\mathbf{X}_p$. It is worth noting that evaluating Eq. (A6) via Eq. (39) with $i=R$ or SM3 result nearly in the same agreement with the exact calculation carried out by MD data, $i=$MD (not shown). Figure 7 also compares the MD results concerning $C_1(t)$ for different molecular weights at $T=1.2$ and for $M=10$ at different temperatures with Eq. (22) with

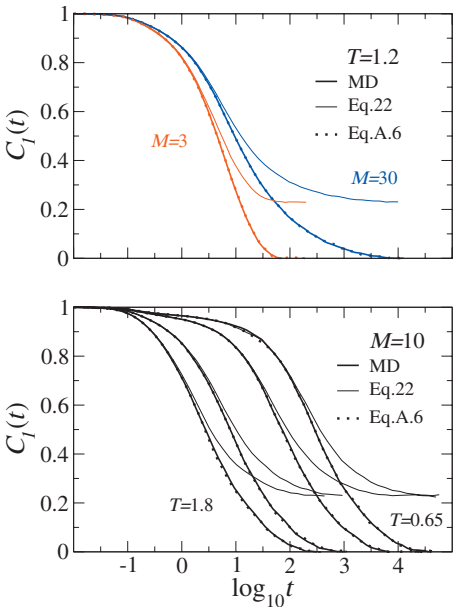

FIG. 7. Rotational correlation functions C_1: comparison of the MD results for $M=3$ and 30 at $T=1.2$ (top) and for $M=10$ at $T=0.65$, 0.75, 1.2, and 1.8 from right to left (bottom) with Eq. (22) with $\ell=1$ and Eq. (A6) with $M_R=M$ (mode correlation functions from simulation data).

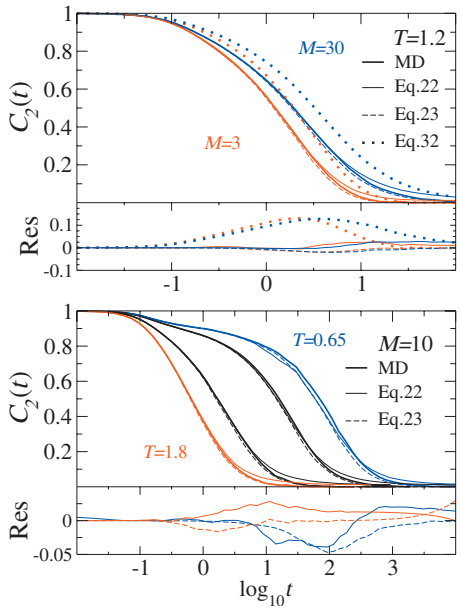

FIG. 8. Rotational correlation functions C_2: comparison of the MD results for $M=3$ and 30 at $T=1.2$ (top) and for $M=10$ at $T=0.65$, 0.75, 1.2, and 1.8 (bottom) with Eq. (22) with $\ell=2$, Eq. (23), and Eq. (32) with $M_R=M$. The bond correlation functions $C_{1,n}(t)$ involved in Eqs. (23) and (32) are evaluated by simulation data. The lower parts of each panel plot the corresponding residuals.

$\ell=1$. By comparing the top panel of Fig. 7 with Fig. 5 (top panel), it is seen that Eq. (22) with $\ell=1$ accounts for the correlation loss up to the end of the intermediate decay regime ($1\lesssim t\lesssim 10$). Notice that: (i) the intermediate decay is *stretched* (see Fig. 5), then Eq. (22) cannot be read as a trivial consequence of the diffusion model predicting *exponential* decays; (ii) the decay is tracked even at low temperatures where the cage effect is more apparent and the non-Gaussian effects are not negligible (see Fig. 1). However, at long times Eq. (22) breaks down in that it does not predict the complete correlation loss but a plateau at $\exp[-\langle\theta^2(\infty)\rangle/2]=\exp[(4-\pi^2)/4]\simeq 0.23$.

Figure 8 compares the MD results concerning $C_2(t)$ for different molecular weights at $T=1.2$ and for $M=10$ at different temperatures with Eq. (22) with $\ell=2$, Eq. (23), and Eq. (32) with $M_R=M$. The top panel of Fig. 8 shows that Eq. (32) agrees poorly with the simulations. This is a little surprising since the latter equation relies on the Gaussian character of the monomer displacement (see Appendix) which is still valid at $T=1.2$, as shown by the small non-Gaussian parameter (see Fig. 1, lower panel). Figure 8 shows better agreement by the two variants of Eq. (21), i.e., Eqs (22) and (23), even at low temperatures where non-Gaussian effects are more apparent. In particular, the agreement of Eq. (22) with $\ell=2$ is much better than for $\ell=1$, owing to the larger decay of $C_2(t)$ for a given mean-square angle $\langle\theta^2(t)\rangle$ spanned by the bond in a time t.

C. Rotational cross-correlation functions

Figure 9 plots the cross-correlation functions $C_{1,\Delta m}$ [Eq. (20)]. The correlations decreases with the bond-bond distance Δm. For a given distance, due to the connectivity, the cross-correlations first increase at short times and then vanish

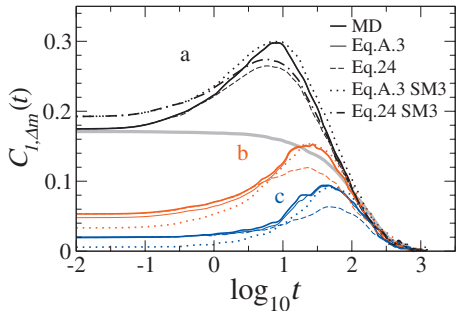

FIG. 9. Rotational cross-correlation functions $C_{1,\Delta m}$ at $T=1.2$ for $M=10$. Curves with a, b, and c labels refer to bond-bond distances $\Delta m=1$, 2, and 3, respectively. The MD results are compared with both Eqs. (24) and (A3) [averaged by using Eq. (A8)]. The latter equations are evaluated by either the MD simulations (thin lines) or the SM3 model (thick lines). The gray curve is evaluated by replacing in Eq. (20) the expression of $C_{1,m,\Delta m}$ as given by Eq. (A3) limiting the sum to the first term only ($p=1$). It is seen that the long-time decay is controlled by the decay of the correlation function of the first Rouse mode ϕ_1 only.

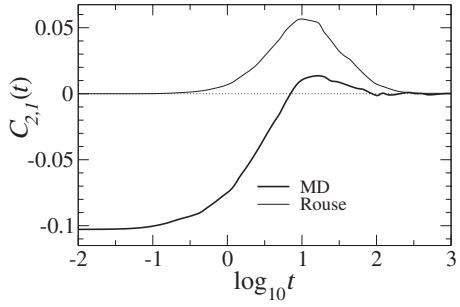

FIG. 10. Rotational cross-correlation function $C_{2,1}$, at $T=1.2$ for $M=10$. The exact MD results are compared with the predictions of the Rouse theory, i.e., Equation (A14) is replaced in Eq. (20) by taking $\phi_p^R(t)$ from the simulations. Note that the "phantom" character of the Rouse chains results in $C_{2,1}^R(0)=0$. The SM3 model predicts $C_{2,1}^{\mathrm{SM3}}(0)=-0.113$ to be compared with $C_{2,1}(0)=-0.103$ from simulations.

when time exceeds the chain rotational correlation time $\sim\tau_1$. The MD results are compared to a number of approximating schemes evaluating $C_{1,m,\Delta m}$ [Eq. (18)]. First, the latter was identified with Eq. (A3), the bond dependence was averaged by Eq. (A8), and the Rouse mode correlation functions were taken directly from the simulations. As it is seen in Fig. 9, the comparison is quite satisfactory since Eq. (A3) relies on the mode orthogonality, which is quite good. We also replaced $\langle \mathbf{X}_p^R(t)\cdot\mathbf{X}_p^R(0)\rangle$ in Eq. (A3) with Eq. (39) with $i=\mathrm{SM3}$. The good agreement shows that the SM3 model well accounts for the excluded volume effects on the static properties. Figure 9 also includes the approximation of $C_{1,m,\Delta m}$ expressed by Eq. (24). The agreement is excellent at short and long times. The discrepancies at intermediate times point to the conclusion that the angle $\beta_{m,\Delta m}$ between $\mathbf{b}_m(0)$ and $\mathbf{b}_{m+\Delta m}(0)$ is partially correlated with the dihedral angle $\phi_{m,\Delta m}(t)$ and the angle $\theta_{m+\Delta m}$ spanned by $\mathbf{b}_{m+\Delta m}$ in a time t. For $\Delta m=1$ the quantities $\langle\cos\beta\rangle$ and $\langle\sin\beta\rangle$ in Eq. (24) were also evaluated by the SM3 model resulting in the dot-dashed line. The partial improvement at intermediate times is counterbalanced by small deviations at short times.

As noted in Sec. III B the "phantom" character of the Rouse chains, due to no account of the excluded volume, implies that their cross-correlations vanish at the initial time, i.e., $C_{\ell,\Delta m}^R(0)=0$ for $\Delta m\neq 0$ [this is seen by evaluating Eq. (A4) at $t=0$]. Figure 9 shows that the weakness of this conclusion in that it shows that $C_{1,\Delta m}(0)\neq 0$ for $\Delta m=1$, 2, and 3. Notice that $C_{1,\Delta m}(t)$, when evaluated via Eqs. (A3) and (A8) and by using the MD results, is coincident with the exact MD results within the errors. This comes as no surprise in that Eq. (A3) relies on the mode-mode orthogonality only and then is virtually exact.

Fig. 10 compares the exact MD evaluation of $C_{2,1}$ with the expectation of the Rouse theory, as given by Eqs. (A14) and (20). Being the former derived on the basis of Eq. (A4) which, in turn, relies on Eq. (37), one finds $C_{2,1}^R(0)=0$. However, the MD simulation yields $C_{2,1}(0)\neq 0$. It is worth noting that $C_{2,1}(0)$ may be evaluated by the SM3 model[52] via Eqs. (17) and (19) by neglecting the m-dependence to yield

$$C_{2,1}^{\mathrm{SM3}}(0)=-0.113, \tag{43}$$

which is in good agreement with $C_{2,1}(0)=-0.103$ from simulations.

VI. CONCLUSIONS

The paper presents a thorough MD study of the segmental (bond) rotational dynamics in a melt of unentangled, linear chains. To single out the connectivity effects, the study considered states with limited deviations from the Gaussian behavior of the linear displacement. Both the self and the cross bond-bond correlations with rank $\ell=1$ and 2 are studied in detail.

For $\ell=1$ (of major interest for dielectric relaxation) the correlation functions are precisely described by expressions involving the correlation functions of the chain modes. This is shown in Figs. 7 and 9 where the general results for the self-correlations, Eq. (A6), and the cross-correlations, Eq. (A3) [averaged by Eq. (A8)], are compared to the simulations, respectively.

Several approximations concerning both the self- and the cross-correlations with $\ell=1$, and 2 are developed and assessed. For $\ell=2$ (involved in NMR, electron paramagnetic resonance, light scattering, and single molecule spectroscopies) a relation between the self-correlations with $\ell=2$ and the ones with $\ell=1$ [Eq. (32)] is derived under the assumption of Gaussian properties of the chain segments (a key hypothesis of the Rouse model). When the relation is compared to the MD results, deviations are noted (see Fig. 8) pointing to limited robustness of Eq. (32) even under small non-Gaussianity. Much better agreement is found by adopting alternative expressions [Eqs. (22) and (23)]. On the other hand, Eq. (22), works only at short times for $\ell=1$ (see Fig. 7). For the cross-correlations with $\ell=1$ the approximate expression. Equation (24) yields excellent agreement at both short and long times (see Fig. 9).

It is found that the Rouse theory, when corrected by stretching the mode-mode correlation functions via Eq. (42) and adopting the simplified description of the excluded volume static effects provided by the SM3 model,[52,53] provides quantitative account of the intermediate- and the long-time

decay of the self-correlations with $\ell=1$. The SM3 model well accounts for the short time cross-correlations for both $\ell=1$ and 2 as well.

The self-correlations are seen to have long-time tails which are little dependent on the temperature, whereas are strongly dependent on the chain length. This feature may provide early signatures of the onset of the reptation dynamics.[16] On the other hand, the cross-correlations evidence the deep impact of the excluded volume effects on the chain dynamics in a much clearer way than the self-correlations and suggest how to investigate in the time-domain the long-range spatial correlations recently reported.[6]

ACKNOWLEDGMENTS

Financial support from MUR within the PRIN project "Aging, fluctuation and response in out-of-equilibrium glassy systems" and FIRB project "Nanopack" as well as computational resources by "Laboratorio per il Calcolo Scientifico," Pisa are gratefully acknowledged.

APPENDIX: ROUSE EXPRESSIONS OF THE SEGMENTAL CORRELATION FUNCTIONS

The Appendix summarizes the derivation of the self- and cross-correlation functions with rank $\ell=1$ and 2 according to the Rouse model. The cross-correlation function $C^R_{1,m,\Delta m}(t)$, Eq. (34), is first considered. By replacing Eq. (5) into Eq. (25), one relates the nth Rouse segment to the chain modes as

$$\mathbf{a}_n(t) = -\frac{4}{a_R}\sum_{p=1}^{M_R-1} c_{n,p}\mathbf{X}^R_p(t), \tag{A1}$$

with

$$c_{np} = \sin\left[\frac{np\pi}{M_R}\right]\sin\left[\frac{p\pi}{2M_R}\right]. \tag{A2}$$

Replacing Eq. (A1) into Eq. (33) and the result into Eq. (34) one finds

$$C^R_{1,m,\Delta m}(t) = \frac{16}{a_R^2}\sum_{p=1}^{M_R-1} c_{m+\Delta m,p}c_{m,p}\langle \mathbf{X}^R_p(t)\cdot\mathbf{X}^R_p(0)\rangle, \tag{A3}$$

$$= \frac{2}{M_R}\sum_{p=1}^{M_R-1}\sin\left[\frac{(m+\Delta m)p\pi}{M_R}\right]\sin\left[\frac{mp\pi}{M_R}\right]\phi^R_p(t). \tag{A4}$$

Equation (A4) is coincident with previous results.[51] The explicit expression of the self-correlation function of the mth segment $C^R_{1,m}(t)$ [see Eq. (28)] is recovered via Eq. (A4) by setting $\Delta m=0$,

$$C^R_{1,m}(t) = \frac{2}{M_R}\sum_{p=1}^{M_R-1}\sin^2\left[\frac{mp\pi}{M_R}\right]\phi^R_p(t). \tag{A5}$$

Notice that $C^R_{1,m}(0)=1$ and $C^R_{1,m}(\infty)=0$.

By replacing Eq. (A3) with $\ell=1$ and $\Delta m=0$ into Eq. (30), a compact expression is obtained for the self-correlation function averaged over all the segments $C^R_1(t)$, which reads

$$C^R_1(t) = \frac{16}{a_R^2(M_R-1)}\sum_{m,p=1}^{M_R-1} c^2_{m,p}\langle \mathbf{X}^R_p(t)\cdot\mathbf{X}^R_p(0)\rangle, \tag{A6}$$

$$= \frac{1}{M_R-1}\sum_{p=1}^{M_R-1}\phi^R_p(t). \tag{A7}$$

Equation (A7) follows by using Eqs. (7), (10), and (11) and is coincident with previous results.[16] By averaging Eq. (A4) over all the segments the expression of $C^R_{1,\Delta m}(t)$ reads

$$C^R_{1,\Delta m}(t) = \frac{1}{M_R-1-\Delta m}\sum_{m=1}^{M_R-1-\Delta m} C^R_{1,m,\Delta m}(t), \tag{A8}$$

$$= \frac{1}{M_R(M_R-1-\Delta m)} \times \sum_{p=1}^{M_R-1}\left\{(M_R-\Delta m)\cos\left[\frac{\Delta mp\pi}{M_R}\right] + \cot\left[\frac{p\pi}{M_R}\right]\sin\left[\frac{\Delta mp\pi}{M_R}\right]\right\}\phi^R_p(t), \tag{A9}$$

which reduces to Eq. (A7) for $\Delta m=0$.

We now consider the cross-correlation function $C^R_{2,m,\Delta m}(t)$. To evaluate Eq. (35), one evaluates the quantity $\langle \chi^{R2}(t)\rangle$ via Eq. (33). Due to the space isotropy one finds

$$\langle \chi^{R2}(t)\rangle = 3\{\langle [a_{m+\Delta m,x}(t)a_{m,x}(0)]^2\rangle + 2\langle a_{m+\Delta m,x}(t)a_{m,x}(0)a_{m+\Delta m,y}(t)a_{m,y}(0)\rangle\}. \tag{A10}$$

For a Gaussian process the identity

$$\langle ABCD\rangle = \langle AB\rangle\langle CD\rangle + \langle AC\rangle\langle BD\rangle + \langle AD\rangle\langle BC\rangle$$

allows to express Eq. (A10) as

$$\langle \chi^{R2}(t)\rangle = \tfrac{4}{3}\langle \mathbf{a}_{m+\Delta m}(t)\cdot\mathbf{a}_m(0)\rangle^2 + \tfrac{1}{3}. \tag{A11}$$

The above expression takes into account also the statistical independence of the different Cartesian components of the vector $\mathbf{a}$, i.e., $\langle a_{m+\Delta m,\alpha}(t_1)a_{m,\beta}(t_2)\rangle=0$ with $\alpha,\beta=x,y,z$, $\alpha\neq\beta$, $\Delta m\geq 0$, and arbitrary t_1 and t_2. For $\Delta m\geq 1$ replacing Eq. (A11) into Eq. (35) yields

$$C^R_{2,m,\Delta m}(t) = \tfrac{4}{3}\langle \mathbf{a}_{m+\Delta m}(t)\cdot\mathbf{a}_m(0)\rangle^2. \tag{A12}$$

Inserting Eqs. (33) and (34) into the above equation proves Eq. (36).

For the self-correlation function $C^R_{2,n}(t)$ the same line of reasoning yields

$$C^R_{2,m}(t) = \langle \mathbf{a}_m(t)\cdot\mathbf{a}_m(0)\rangle^2. \tag{A13}$$

Inserting Eq. (28) into the above equation proves the equality $C^R_{2,n}(t)=C^R_{1,n}(t)^2$, i.e., Eq. (31). Replacing Eq. (A5) into the latter equality relates $C^R_{2,n}(t)$ to the correlation functions of the Rouse modes. A similar task may be accomplished also

for the cross-correlation function $C^R_{2,m,\Delta m}(t)$. By replacing Eq. (A4) into Eq. (36) one gets

$$C^R_{2,m,\Delta m}(t) = \frac{16}{3M_R^2}\left\{\sum_{p=1}^{M_R-1} \sin\left[\frac{(m+\Delta m)p\pi}{M_R}\right]\sin\left[\frac{mp\pi}{M_R}\right]\phi^R_p(t)\right\}^2. \tag{A14}$$

If the self-correlation function $C^R_{2,n}(t)$ is averaged over all the segments a compact expression for $C^R_2(t)$ is obtained from Eq. (32) and Eq. (A5) as

$$C^R_2(t) = \frac{1}{2M_R(M_R-1)}\sum_{p,q=1}^{M_R-1} \sigma_{M_R,p,q}\phi^R_p(t)\phi^R_q(t), \tag{A15}$$

with

$$\sigma_{M_R,p,q} = 2 + \delta_{pq} + \delta_{p+q,\ M_R}. \tag{A16}$$

An analytical explicit expression for $C^R_{2,\Delta m}(t)$ may be also derived. However, it is quite long and then of limited interest.

[1] N. G. McCrum, B. E. Read, and G. Williams, *Anelastic and Dielectric Effects in Polymeric Solids* (Dover, New York, 1991).
[2] K. Schmidt-Rohr and H. W. Spiess, *Multidimensional Solid-State NMR and Polymers* (Academic, London, 1994).
[3] *Spin Labeling: Theory and Applications*, edited by L. J. Berliner (Academic, New York, 1976); *Biological Magnetic Resonance*, edited by L. J. Berliner and J. Reuben (Plenum, New York, 1989), Vol. 8.
[4] B. J. Berne and R. Pecora, *Dynamic Light Scattering* (Wiley, New York, 1975).
[5] W. P. Ambrose, P. M. Goodwin, J. H. Jett, A. Van Orden, J. H. Werner, and R. A. Keller, Chem. Rev. **99**, 2929 (1999).
[6] J. P. Wittmer, H. Meyer, J. Baschnagel, A. Johner, S. Obukhov, L. Mattioni, M. Muåller, and A. N. Semenov, Phys. Rev. Lett. **93**, 147801 (2004).
[7] A. V. Lyulin, N. K. Balabaev, and M. A. J. Michels, Macromolecules **35**, 9595 (2002).
[8] K. Karatasos and D. B. Adolf, J. Chem. Phys. **112**, 8225 (2000).
[9] Y. H. Lin and Z. H. Luo, J. Chem. Phys. **112**, 7219 (2000).
[10] W. Paul and H. L. Frisch, Phys. Rev. E **60**, 697 (1999).
[11] J. P. Gao and J. H. Weiner, Macromolecules **29**, 6048 (1996).
[12] C. Bennemann, W. Paul, J. Baschnagel, and K. Binder, J. Phys.: Condens. Matter **11**, 2179 (1999).
[13] J. Baschnagel and F. Varnik, J. Phys.: Condens. Matter **17**, R851 (2005).
[14] Y. N. Kaznessis, D. A. Hill, and E. J. Maginn, Macromolecules **32**, 6679 (1999).
[15] R. Faller, M. Putz, and F. Müller-Plathe, Int. J. Mod. Phys. C **10**, 355 (1999); R. Faller, Dissertation, Universität Mainz, 2000.
[16] T. Kreer, J. Bashnagel, M. Müller, and K. Binder, Macromolecules **34**, 1105 (2001).
[17] A. Barbieri, E. Campani, S. Capaccioli, and D. Leporini, J. Chem. Phys. **120**, 437 (2004).
[18] A. Barbieri, D. Prevosto, M. Lucchesi, and D. Leporini, J. Phys.: Condens. Matter **16**, 6609 (2004).
[19] P. E. Rouse, J. Chem. Phys. **21**, 1272 (1953).
[20] M. F. Gelin and D. S. Kosov, J. Chem. Phys. **125**, 054708 (2006).
[21] C.-Y. Lu and D. A. Vanden Bout, J. Chem. Phys. **125**, 124701 (2006).
[22] J. D. Ferry, *Viscoelastic Properties of Polymers*, 3rd ed. (Wiley, New York, 1980).
[23] M. Doi and S. F. Edwards, *The Theory of Polymer Dynamics* (Clarendon, Oxford, 1986).
[24] G. Strobl, *The Physics of Polymers* (Springer, New York, 1997).
[25] T. P. Lodge, N. A. Rotstein, and S. Prager, Adv. Chem. Phys. **79**, 1 (1990).
[26] W. Paul, G. D. Smith, D. Y. Yoon, B. Farago, S. Rathgeber, A. Zirkel, L. Willner, and D. Richter, Phys. Rev. Lett. **80**, 2346 (1998).
[27] G. D. Smith, W. Paul, M. Monkenbusch, and D. Richter, J. Chem. Phys. **114**, 4285 (2001).
[28] M. Doxastakis, D. N. Theodorou, G. Fytas, F. Kremer, R. Faller, F. Müller-Plathe, and N. Hadjichristidis, J. Chem. Phys. **119**, 6883 (2003).
[29] D. S. Pearson, G. Ver Strate, E. von Meerwall, and F. C. Schilling, Macromolecules **20**, 1133 (1987).
[30] D. S. Pearson, L. J. Fetters, W. W. Greassley, G. Ver Strate, and E. von Meerwall, Macromolecules **27**, 711 (1994).
[31] H. Tao, T. P. Lodge, and E. D. von Meerwall, Macromolecules **33**, 1747 (2000).
[32] K. Binder, J. Baschnagel, and W. Paul, Prog. Polym. Sci. **28**, 115 (2003).
[33] M. Guenza, Phys. Rev. Lett. **88**, 025901 (2001).
[34] W. Paul, Chem. Phys. **284**, 59 (2002).
[35] W. Paul and G. D. Smith, Rep. Prog. Phys. **67**, 1117 (2004).
[36] C. Bennemann, J. Baschnagel, W. Paul, and K. Binder, Comput. Theor. Polym. Sci. **9**, 217 (1999).
[37] K. Kremer and G. S. Grest, J. Chem. Phys. **92**, 5057 (1990).
[38] J. Baschnagel, C. Bennemann, W. Paul, and K. Binder, J. Phys.: Condens. Matter **12**, 6365 (2000).
[39] V. A. Harmandaris, M. Doxastakis, V. G. Mavrantzas, and D. N. Theodorou, J. Chem. Phys. **116**, 436 (2002).
[40] M. Mondello, G. S. Grest, E. B. Webb, and P. Peczak, J. Chem. Phys. **109**, 798 (1998).
[41] A. Kopf, B. Dunweg, and W. Paul, J. Chem. Phys. **107**, 6945 (1997).
[42] M. Aichele and J. Baschnagel, Eur. Phys. J. E **5**, 229 (2001).
[43] J. T. Padding and W. J. Briels, J. Chem. Phys. **115**, 2846 (2001).
[44] C. Yeung and B. Friedman, J. Chem. Phys. **122**, 214909 (2005).
[45] S. H. Chong and M. Fuchs, Phys. Rev. Lett. **88**, 185702 (2002).
[46] P. H. Verdier, J. Chem. Phys. **45**, 2118 (1966).
[47] Y.-H. Lin, *Polymer Viscoelasticity* (World Scientific, Singapore, 2003).
[48] L. Alessi, L. Andreozzi, M. Faetti, and D. Leporini, J. Chem. Phys. **114**, 3631 (2001).
[49] R. A. Orwell and W. H. Stockmayer, Adv. Chem. Phys. **15**, 305 (1969).
[50] P. H. Verdier, J. Chem. Phys. **52**, 5512 (1970).
[51] See Appendix 4.I of Ref. 23.
[52] D. Molin, A. Barbieri, and D. Leporini, J. Phys.: Condens. Matter **18**, 7543 (2006).
[53] A. Ottochian and D. Leporini, J. Non-Cryst. Solids **353**, 3879 (2007).
[54] M. P. Allen and D. J. Tildesley, *Computer Simulation of Liquids* (Clarendon, Oxford, 1987).
[55] C. De Michele and D. Leporini, Phys. Rev. E **63**, 036702 (2001).